ELSEVIER

Contents lists available at ScienceDirect

# Biosensors and Bioelectronics: X

journal homepage: www.journals.elsevier.com/biosensors-and-bioelectronics-x



# Towards monitoring of critical illness via the detection of histones with extended gate field-effect transistor sensors

Hayley Richardson <sup>a,b</sup>, Jeffrey Barahona <sup>b</sup>, Greg Medwig <sup>b</sup>, Angela Johns <sup>b</sup>, Lina M. Acosta Pérez <sup>c</sup>, Koji Sode <sup>c</sup>, Michael Daniele <sup>b,c</sup>, Francis J. Miller <sup>d,e</sup>, Edgar Lobaton <sup>b</sup>, Spyridon Pavlidis <sup>b,\*</sup>

- <sup>a</sup> Department of Materials Science and Engineering, North Carolina State University, Raleigh, NC, 27695, USA
- <sup>b</sup> Department of Electrical and Computer Engineering, North Carolina State University, Raleigh, NC, 27695, USA
- c Joint Department of Biomedical Engineering, University of North Carolina at Chapel Hill and North Carolina State University, Chapel Hill, NC, 27599, USA
- d Department of Medicine, Veterans Affairs Tennessee Valley Medical Center, Nashville, USA
- <sup>e</sup> Department of Medicine, Vanderbilt University Medical Center, Nashville, USA

#### ARTICLE INFO

# Keywords: Histone Aptamer Multiple organ dysfunction syndrome Extended gate field-effect transistor Surface plasmon resonance Self-assembled monolayer

#### ABSTRACT

Extracellular histone proteins in the blood indicate a heightened risk of morbidity after trauma or in major illnesses such as sepsis. We present the development of an aptasensor for histone detection with an extended gate field-effect transistor (EGFET) configuration, which benefits from low power consumption, rapid response, and compatibility with miniaturized gold electrodes. Histones have a high isoelectric point and charge density, which cause them to physically adsorb to non-specific elements of the sensor that have available electrostatic charges. To combat this, the sensing surface is formed with a thiol-modified, high-affinity and histone-specific RNA aptamer sequence and by co-immobilizing with poly(ethylene glycol) methyl ether thiol (PEG) as a blocking agent. Surface plasmon resonance (SPR) is used to analyze aptamer and PEG immobilization strategies, confirm histone binding, and calculate kinetic binding constants. Through comparison of different blocking agents and time-dependent preparation, the ideal equilibrium dissociation constant (KD) is estimated to be below 200 pM, which is the upper range of extracellular histone concentrations in critically ill patients with high mortality. The EGFET sensitivity of the optimized aptasensor is 6.65 mV/decade concentration change for histone H4 with a physiologically relevant 5 pM limit of detection. Selectivity tests with 100 nM bovine serum albumin (BSA) demonstrate a signal response that is 13-fold smaller than for histones. This EGFET aptasensor platform is suitable for future point-of-care monitoring of histone levels in critically ill patients, thus permitting the early detection of increased risk and the need for more aggressive interventional measures to prevent mortality.

# 1. Introduction

When the body experiences trauma or major illness, damaged cells release their nuclear contents, including histone proteins, into the extracellular space and circulation. Extracellular histone proteins, particularly H3 and H4, cause direct cellular toxicity and elicit inflammatory responses. Extracellular histones are mediators of acute respiratory distress syndrome (ARDS) and multiple organ dysfunction syndrome (MODS) (Szatmary et al., 2018), (Xu et al., 2009), (Lei et al., 2023). Thus, extracellular histone levels are not only a biomarker of illness severity but also directly mediate tissue damage and associated morbidity and mortality.

Monitoring circulating histone levels in critically ill patients would improve the early recognition of increased risk. Normal histone concentrations in serum are below 0.6 ng/mL (50 pM) and can spike to 3 ng/mL (200 pM) in patients after trauma or sepsis (Szatmary et al., 2018), (Xu et al., 2009), (Lei et al., 2023). Current detection techniques for MODS and ARDS rely on clinical scores to predict mortality (Marshall et al., 1995), (Luo et al., 2017). Prediction scores are dynamic calculations that assist medical providers in making decisions on care but are vulnerable to human subjectivities, multiple and complex metrics, and vary depending on the mechanism of illness (Rapsang and Shyam, 2014), (Arina et al., 2023). Furthermore, clinical indicators often reflect late manifestations of illness severity. Delays in diagnosis or

<sup>\*</sup> Corresponding author. North Carolina State University, Raleigh, NC, 27695, USA. *E-mail address:* spavlidis@ncsu.edu (S. Pavlidis).

inability to recognize the failure of therapies are associated with increased mortality in this patient population. The availability of a single, objective, and quantitative assay of illness severity would allow earlier clinical diagnosis and directed treatment. We propose that this goal can be accomplished by developing a point-of-care (POC) sensor for detecting circulating histones.

An emerging transduction method for charge-based quantification of analyte concentrations for POC testing is the use of extended gate field-effect transistor (EGFET) platforms (Tarasov et al., 2016). EGFET sensors have accomplished reliable signal generation based on the charge transfer between target analytes and recognition elements on electrode surfaces (Hatada et al., 2024), (Janićijević et al., 2023). Potentiometric transduction via EGFET sensors will capture net charge changes of the histone binding complex through the systems' low-noise sensitivity while combining inexpensive, reusable electronics with consumable biosensors (Chu et al., 2017). This method is advantageous towards POC testing due to these aforementioned benefits, in addition to low power requirements and low sample consumption.

In the EGFET setup, a functionalized gold working electrode (WE) is connected to the gate of a metal-oxide-semiconductor field-effect transistors (MOSFET) (Fig. S1). Analytes, ions, or pH charges change the surface potential of the extended gate WE and therefore the current in the MOSFET channel. By comparing the gate-to-source voltage ( $V_{\rm GS}$ ) at the same drain-to-source current ( $I_{\rm DS}$ ) for different solutions, an effective threshold voltage ( $V_{\rm TH}$ ) shift is tracked, which is indicative of the charge-based changes at the WE's surface (Kaisti, 2017).

A major challenge of this proposed histone-target sensor system is overcoming the dense positive charges of histone proteins, due to their high isoelectric point and molecular weight (pI = 11 and MW = 11–22 kDa) (Gargano et al., 2018). This threatens potential non-specific adhesion (NSA) of histones to electrostatically charged species, like exposed gold on the sensor surface, which reduces the specificity of the sensor's response. Aptamer sequences present an innovative approach with great capabilities towards POC sensing due to their high affinity to a myriad of targets. Using aptamers as the functionalized surface has advantages such as their small size, which allows them to target analytes with high charge densities without sacrificing the proper conformation for binding and high selectivity to limit NSA (Liu et al., 2021).

Recently, RNA aptamer sequences were developed towards possible treatment of MODS in murine models (Lei et al., 2023), (Urak et al., 2019). Sequence "KU7" had the best affinity measurements in a double-filter binding assay for human histone H4 and for calf thymus histone (CTH), at 0.68 nM and 4.109 nM, respectively (Urak et al., 2019). Using surface plasmon resonance (SPR), significant binding activity was also reported between solution-phase KU7 aptamers and immobilized histones, with a calculated dissociative binding constant of  $K_{\rm D}=4.01\pm0.4$  nM for H4 histones and  $K_{\rm D}=5.6\pm0.1$  nM for CTH (Urak et al., 2019). Specificity of the aptamer was observed through a lack of significant binding to serum proteins in the performed selection procedure, assays, and SPR analysis (Urak et al., 2019).

Our group has previously demonstrated the concept of immobilizing KU7 onto gold for future POC detection of histones (Richardson et al., 2022). First, SPR was performed on surfaces with and without KU7 immobilized. Statistically significant differences in binding response between the active and control surfaces were demonstrated through these experiments. However, the partial accumulation of histone proteins on the control surfaces without KU7 were an initial result suggesting that proper passivation with an additional chemical was important to achieve a specific binding signal. Two-electrode potentiometric experiments (i.e., not EGFET) were executed on commercial gold electrodes to compare the binding response of three different surfaces without KU7: cleaned gold; mercapto-1-hexanol (MCH); and poly (ethylene glycol) methyl ether thiol (PEG). PEG had the least amount of bound CTH and was therefore used in combination with the KU7 aptamer for an ideal sensor co-monolayer. A potentiometric response was measured for concentrations of CTH from 1.56 nM to 1 µM in buffer

and achieved a logarithmic sensitivity of 7.8 mV/decade concentration change. At the time, the report of a sensor response for a CTH concentration of less than 2 nM represented an order of magnitude improvement compared to concentrations investigated in prior potentiometric sensors for H4 detection that used a different anti-histone aptamer sequence (Goda and Miyahara, 2020).

Here, we employ the aforementioned aptamer sequence to detect histones in solution with an improved platform utilizing an EGFET system. With aptamers, the binding complex and charge exchange is in close proximity to the surface (Fig. 1), which ameliorates electron transfer by modulating the surface potential of the metal sensor (Cho et al., 2009). Since one terminal end of the aptamer chain is anchored to the sensor surface, optimizing the functionalization process and sensing environment is necessary for the optimal tertiary structure in the binding complex (Daniel et al., 2013). Tuning these parameters in buffer will help achieve sensitivity and selectivity in more challenging high ionic strength media (Cao et al., 2023). To corroborate the EGFET sensor results, a comprehensive suite of SPR experiments was performed to explore more system parameters than previously considered (Richardson et al., 2022).

The rest of this article is organized as follows: Section 2 describes the materials and sensing methods used, which include SPR and EGFET sensing. Sections 3 and 4 present the results and accompanying discussion for the characterization of the immobilization process, SPR-based detection of histones using different spacer molecules, and EGFET sensing measurements that culminate in the physiologically relevant demonstration of pM-level histone detection.

#### 2. Materials & methods

#### 2.1. Gold working electrode fabrication and cleaning for EGFET sensing

Unless otherwise specified, chemical reagents were purchased from MilliporeSigma (Missouri, USA). For validation processes and EGFET sensing experiments,  $1.0\times0.6$  cm working electrodes (WE) were fabricated in the NC State Nanofabrication Facility (NNF) by electron-beam evaporation of 20/100 Ti/Au on Si wafers with a 300 nm thick thermal oxide (Fig. S1). Electrode preparation was done with solvent rinsing, O<sub>2</sub> plasma ashing, and electrochemical potential cycling to limit surface defects, oxide formation, and exposure to debris as much as possible (Xiao et al., 2007). Potential cycling was performed on a Gamry 600+ Potentiostat with cyclic voltammetry (CV) from -1.0 V to +1.3 V at 100 mV/s for 12 scans in 0.5 M  $_{12}$ SO<sub>4</sub>.

# 2.2. Aptamer and spacer molecule immobilization

The anti-histone RNA aptamer sequence ("KU7") has the following RNA sequence: 5'- GGG AGG ACG AUG CGG ACU GGU GAA GGG AGG UAC UGC AGA CGA CUC GCC CGA - 3' (Urak et al., 2019). A 5' Thiol Modifier C6 S-S modification was added to the aptamer to enable gold-thiol assembly. Immobilization buffer (10 mM Tris, 0.1 mM EDTA) and thiolated RNA aptamer solutions were designed and purchased through Integrated DNA Technologies (Iowa, USA). (2-carboxyethyl)phosphine (TCEP) reduced the disulfide bond found on the 5' end prior to self-assembly formation on gold. For EGFET sensing, the aptamer self-assembled monolayer (SAM) was formed overnight under ambient condition by submerging cleaned gold electrodes in 1 µM thiol-aptamer solution in immobilization buffer (Richardson et al., 2021). Separately, 1 mM 6-mercapto-1-hexanol (MCH) or poly(ethylene glycol) methyl ether thiol (PEG) spacer molecules were backfilled for 1 h before testing. In addition to electrochemically cleaning the gold electrodes, CV was also performed to validate the SAM formation. A redox solution of 1 M KCl and 10 mM K<sub>3</sub>[Fe(CN)<sub>6</sub>]/K<sub>4</sub>[Fe(CN)<sub>6</sub>] was used to track the redox potential of the surface reactions. The KCl curves were measured from -0.5 V to 0.5 V for 5 scans at 100 mV/s.

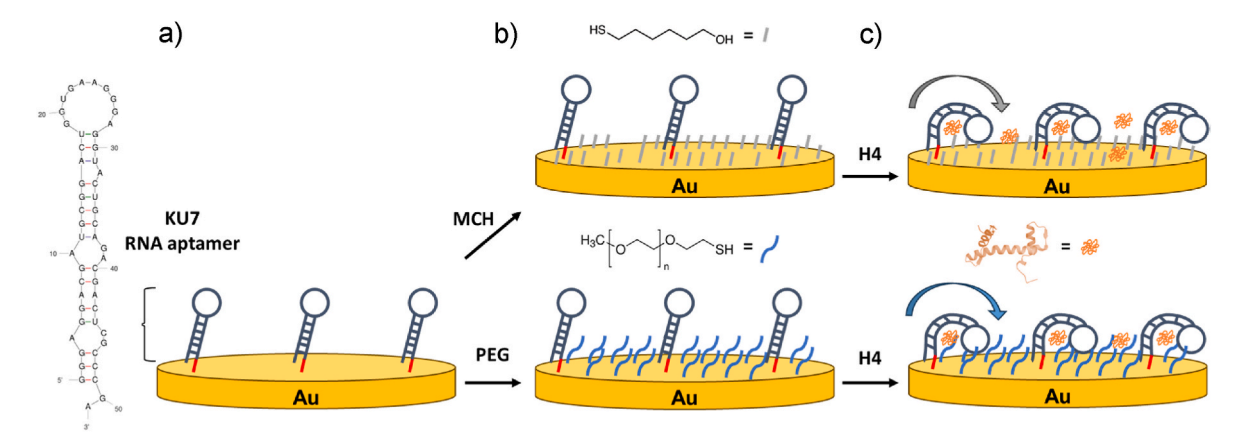


Fig. 1. Sensor functionalized and binding mechanisms. a) Immobilization of KU7 aptamer sequence (blue-gray) with thiol moiety (red) by self-assembly on gold electrodes. Aptamer secondary structure was modeled with Mfold web server (Zuker, 2003). b) MCH or PEG spacer molecule immobilization by backfilling available gold surface. c) Binding of H4 to aptamer, which causes conformational change and modified charge transfer to the electrode surface. NSA is represented by H4 adhesion to MCH or PEG. (For interpretation of the references to colour in this figure legend, the reader is referred to the Web version of this article.)

Both *in-situ* (i.e. flowed through the microfluidics of the SPR instrument) or *ex-situ* (i.e. stagnant in a benchtop setup) immobilization were explored for SPR measurements. *In-situ* immobilization was executed by flowing the 1  $\mu$ M thiol-aptamer solution over a blank gold surface on the active channel for 15 h at 1  $\mu$ L/min. This was followed by flowing 1 mM MCH or PEG over both the active and control channels for 5 h at 1  $\mu$ L/min (Richardson et al., 2022). For *ex-situ* immobilization, electrodes were functionalized in petri dishes for the same time scales, and then loaded into the SPR instrument for subsequent analyte testing.

#### 2.3. Surface plasmon resonance binding

Human histones H4 were purchased from New England Biolabs (Massachusetts, USA). Bovine serum albumin (BSA) and calf thymus histones (CTH) were tested in both SPR and EGFET platforms at similar concentration ranges to H4 histones to test the selectivity and specificity of the aptasensor surface. SPR chips from the SIA Au Kit (# BR100405) and HBS-EP + running buffer (0.1 M HEPES, 1.5 M NaCl, 0.03 M EDTA and 0.5% v/v Surfactant P20) were purchased from Cytiva for use in a Biacore T200 instrument (Massachusetts, USA). SPR chips were cleaned with a standard piranha solution of 3:1 mix of H<sub>2</sub>SO<sub>4</sub>:H<sub>2</sub>O<sub>2</sub> for 30 min prior to mounting and insertion into the SPR instrument. SPR experiments were performed following an established titration procedure for human histones H4 as the target analyte and BSA as an orthogonal control protein in running buffer (Richardson et al., 2022). Peak response units (RU) were selected at the end of the 180s association phases. Regeneration between concentrations was performed with a weak acid solution of 10 mM HCl for 60 s at 30  $\mu$ L/min. For the first experiment with MCH, a dilution series in molar concentration was done with H4, CTH, and BSA. For later experiments with PEG, to best compare RU values for analytes of such different molecular weight, some dilution series were done in  $\mu g/mL$  (Figs. S2–S6).

#### 2.4. EGFET platform, pH and ionic sensing, and histone sensing

Ionic strength, pH, and analyte sensing were all performed with similar protocols in the EGFET platform with commercial off the shelf (COTS) silicon MOSFETs (ZVNL110A) from Diodes Incorporated (Texas, USA). The electropolymerization of a thin film of polyaniline (PANI) on the fabricated gold WE was done to create microfluidic compatible pH-sensitive electrodes adapted from the cited procedure (Bessière et al., 2004). With the Gamry 600+ Potentiostat, 30 CV cycles at 100 mV/s from -0.2 V to 1.0 V were performed in a three-electrode cell with a platinum wire counter electrode and a chlorinated silver wire reference electrode (RE) in an aniline solution. Then, PANI electrodes were cured

at 80 °C for 5 min and stored with desiccant until use. For pH and ionic strength experiments, a chlorinated silver wire RE was created by electrodepositing Cl<sup>-</sup> from 1 M HCl by reaction with a 9V battery.

For histone electrochemical sensing, a double junction Ag/AgCl RE was used from Pine Research (North Carolina, USA). A microfluidic platform from Micrux Technologies (Gijón, Spain) was adopted to limit the exposed area of the working electrodes to 0.6 cm<sup>2</sup> using 0.5 mL of solution while testing (Fig. S1b).

A blank electrolyte was allowed to equilibrate with the surface for 10 min before EGFET measurements were performed. For each measurement, four sweeps were performed from  $V_{GS} = -0.2 \text{ V}-1.0 \text{ V}$  and  $V_{DS} = 0.5 \text{ V}$  and the  $I_{DS}$  recorded. Then, 10 more minutes passed before the next measurement was taken. In ionic strength and analyte sensing, baseline stability with only buffer was measured until  $\pm 1$  mV was obtained. Measurements were taken twice for each analyte concentration in order to achieve a standard deviation for eight V<sub>GS</sub> sweeps and ensure precise voltage readings. The differential was calculated between the stabilized buffer  $V_{GS}$  value, and the average of the eight concentration sweeps to show the voltage shift by analyte binding and plotted as the absolute value of the potential change versus the analyte concentration on a logarithmic scale. To understand selectivity of the sensor, BSA was tested at one high concentration. Commercial pH buffers 4, 7, and 10 were tested for pH. The ionic strength experiments were done with phosphate buffer saline with chlorine ions (PBS: 7.5 mM Na<sub>2</sub>HPO<sub>4</sub>, 2.5 mM NaH<sub>2</sub>PO<sub>4</sub>, 2.7 mM KCl and 137 mM NaCl) at pH 7.4 and diluted with DIH2O for the weaker strengths. 0.1x, 0.2x, and 1.0x strength PBS were tested.

#### 3. Results

#### 3.1. Functionalization of aptasensor

Direct immobilization of the aptamer sequence to the gold was achieved through the C6 S–S linker to maintain a small distance between the aptamer-histone binding interaction and the electrode surface (Fig. 1). Ideally, a continuous SAM is formed during immobilization. However, atomic scale defects in the metal surface can alter the ordering of SAM and create defects like vacancies, bilayer formation, or tangled chains (Josephs and Ye, 2013). To better understand the topography of the initial gold surface, atomic force microscopy (AFM) studies were done to compare the relative roughness of the commercial SPR chips and fabricated WEs for EGFET sensing. (Fig. 2a and b). The EGFET WE and SPR gold chips were cleaned using the preparation methods described in Section 2.1 and 2.3, respectively. The roughness and topology of the gold were measured using a scan size of 6.25 µm² at 1.00 Hz scan rate to

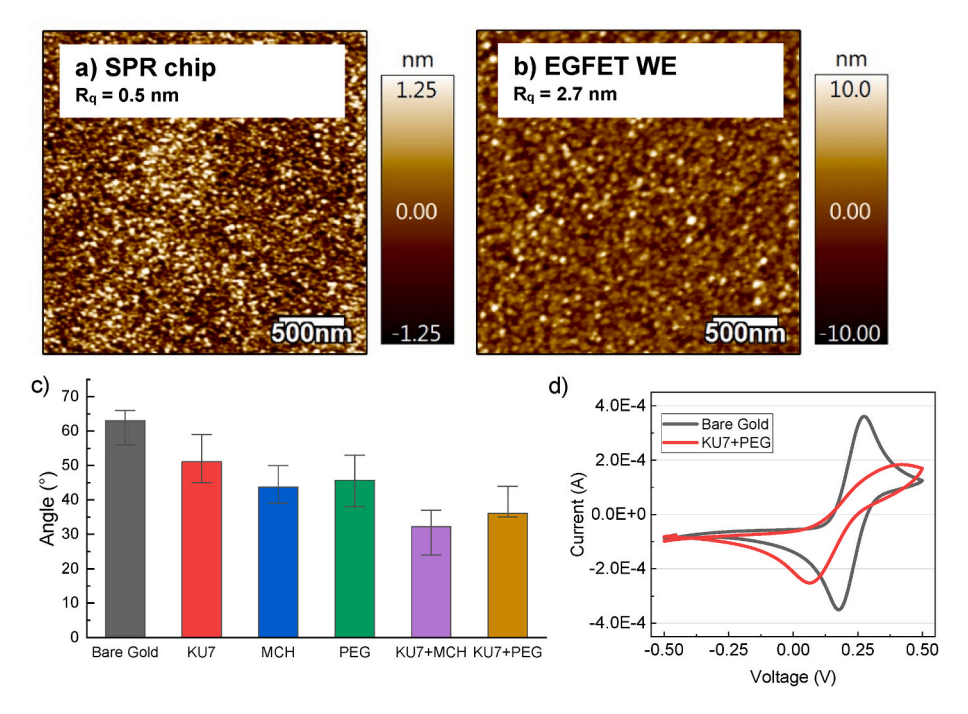


Fig. 2. a) AFM results for SPR chip and b) fabricated EGFET WE's. c) Angle (°) of water droplet on the bare EGFET WE, or with aptamer, alkanethiol, or co-SAM modification. d) Voltammogram comparing the redox peaks of the KCl solution and EGFET WE post-clean and after functionalizing with histone-aptamer and PEG.

calculate root-mean-square roughness ( $R_q$ ). The  $R_q$  of the EGFET WE was approximately five-fold larger than that of the commercial SPR chip, which was anticipated since the latter employs a thinner metal stack and undergoes smoothening steps. Nonetheless, it is sufficiently smooth for EGFET sensing (Purwidyantri et al., 2015).

Contact angle measurements were done with water (surface tension,

 $\gamma=72$  mN/m), with 10 individual 30  $\mu L$  drops added to the surface of clean EGFET WE, measured, then dried with air. The average of n=10 and error bars are plotted in Fig. 2c. The contact angle of gold was within the expected range of 60–70° (Erb, 1968). Surfaces with SAMs measured a lower contact angle than that of bare gold, suggesting that the thiol-molecules immobilized to the surface and withstood repeated wash

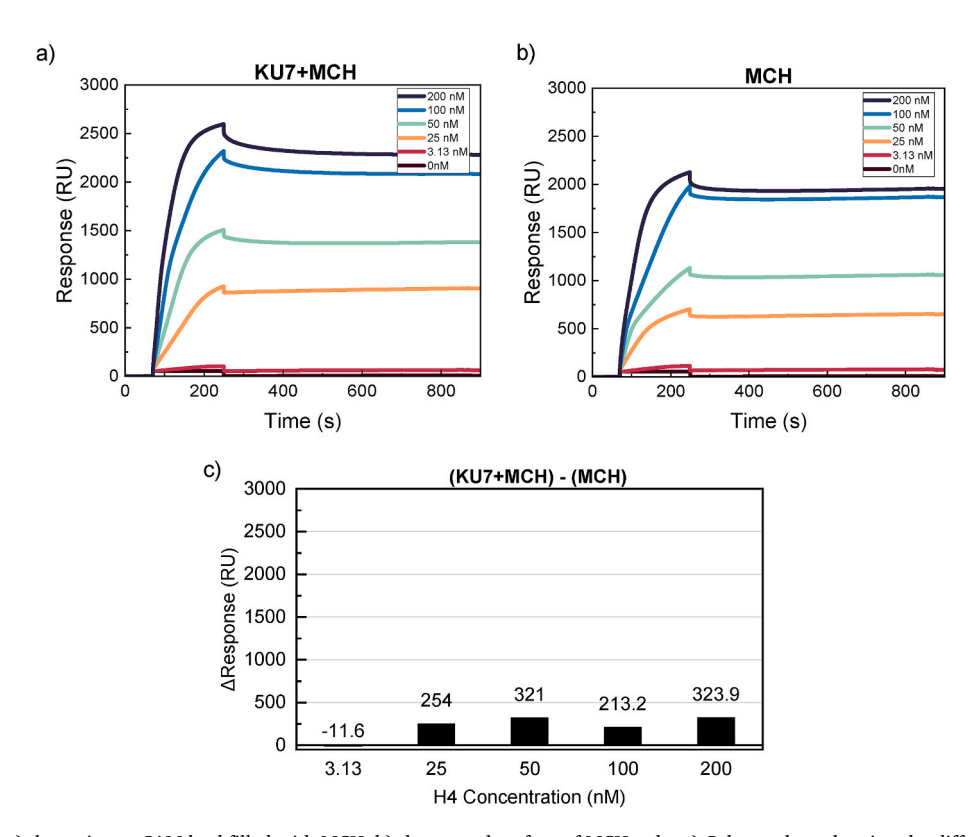


Fig. 3. Sensorgrams for a) the active co-SAM backfilled with MCH, b) the control surface of MCH only. c) Column chart showing the differential response between the aforementioned active and control surfaces.

and dry steps (Bain et al., 1989), (Nuzzo and Allara, 1983). Focusing on the histone aptamer surfaces with spacers, the measured angle was different depending on whether only the aptamer, or aptamer plus spacer molecules (either MCH or PEG) were immobilized. The wettability was different due to differences in charge rearrangement in the co-SAM. This was an initial implication that the spacer molecule impacts the interaction of the aptamer with its environment.

In Fig. 2d., the peak shape of the voltammogram for the bare gold electrode illustrates the expected response of the reversible redox couple,  $[\text{Fe}(\text{CN})_6]^{4-/3}$ . Ferrocyanide/ferricyanide complexes are a standard electrochemical method to analyze differences in electron transfer of surfaces with oligonucleotides through techniques such as CV or electrochemical impedance spectroscopy (Boon et al., 2000), (Li et al., 2023). For the functionalized electrodes, the cyclic voltammogram shows a reduced current and broadening of the redox peaks, indicative of a surface-limiting effect on the charge transfer between the redox agent in the electrolyte and electrode (Eckermann et al., 2010). These results point to the successful functionalization of the histone-binding aptamer and PEG, supporting the interpretation that

surface functionalization impacts the electrochemical reaction rate.

#### 3.2. SPR sensorgrams and kinetics results

SPR measurements were conducted to compare the impact of spacer molecule selection on the NSA. MCH-backfilled sensors were tested first following the *in-situ* immobilization protocol previously mentioned. Fig. 3 shows transient sensorgrams for an active flow cell (Fig. 3a: "KU7 + MCH") and a control flow cell (Fig. 3b: "MCH Only"). H4 showed more binding to the KU7+MCH surface, but there was still significant NSA of H4 to the MCH-only surface. At 200 nM H4, the calculated aptamer-only response – calculated as the differential between the two flow cells – was less than 20% response of the total measured active flow cell's response (Fig. 3c). This suggests that a major portion of the active surface's binding result cannot be singularly attributed to that of the histone-specific aptamer, thus making MCH a poor choice for the spacer molecule in the aptasensor system.

For comparison, *in-situ* functionalization was performed to inspect the behavior of PEG as a spacer molecule (Fig. 4a). While the measured

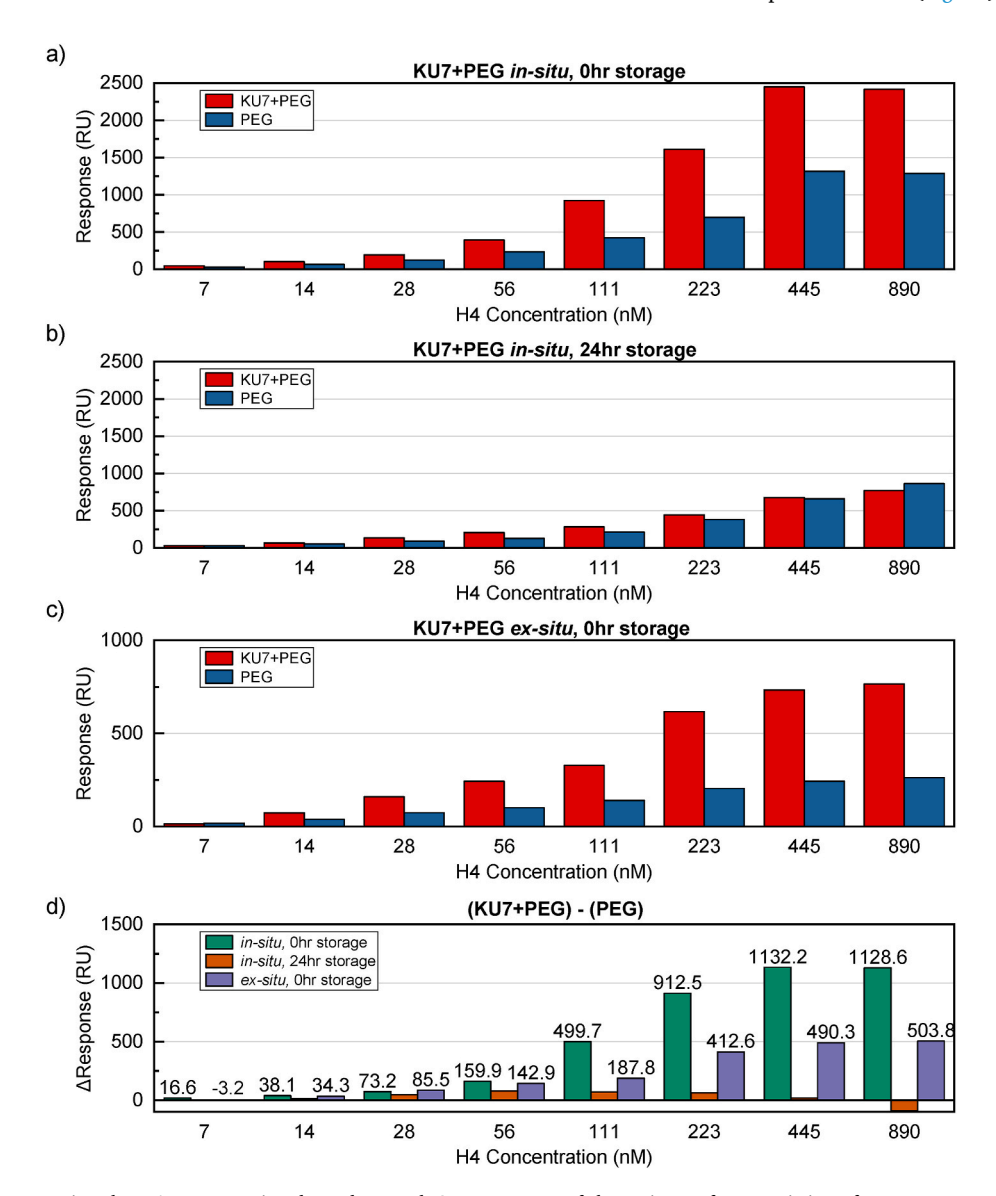


Fig. 4. Column charts comparing the H4 concentration-dependent peak SPR responses of the active surface consisting of an aptamer + PEG co-SAM versus the control, PEG-only surface. The chips were prepared a) *in-situ* immobilization followed by immediate testing, b) *in-situ* immobilization followed by 24-hr storage prior to testing and c) ex-situ immobilization followed by immediate testing. d) The differential peak SPR response of the aforementioned surfaces. RU values are shown above columns for *in-situ*, 0hr storage and *ex-situ* 0hr storage for ease of comparison.

response of the active "KU7+PEG" surface was similar in maximum response to that of the "KU7+MCH" surface, the differential (i.e., active control) response was much larger when PEG was used (Fig. 4d). For example, the differential response for the MCH-based surfaces was 323.9 RU when exposed to an H4 concentration of 200 nM. The differential response in the PEG-based surfaces when exposed to 223 nM of H4, by comparison, was 913 RU, or almost three times larger. This was because the PEG-only surface possessed significantly smaller non-specific interactions with H4. At 223 nM, the PEG-only surface had a RU of 689, which was much less than 200 nM H4 on the MCH-only surface with 2126 RU. While both control surfaces demonstrated some NSA of histones to non-specific electrostatically charged elements on the surface, the response was lower when using the PEG-only control surface. This motivates the use of PEG as a spacer molecule to reduce unwanted interactions based on charge. It is additionally worth noting that 0 and 0.625 µg/mL concentrations were repeated (not shown) to observe any effects from repeated cycles with regeneration. It was thus confirmed that regeneration does not degrade the chemical monolayer on the surface due to similar peak RU values.

Further SPR experiments were conducted to investigate major variables that may influence immobilization and sensor performance when PEG was used as a spacer. For example, prior reports of aptasensors have demonstrated that a 24-h stabilization period improves binding performance (Nagata et al., 2023). Thus, SPR chips that were prepared via *in-situ* immobilization were stored in HBS-EP + prior to testing. The response of both the KU7+PEG and PEG-only channels are shown in Fig. 4b, and it can be seen that the differential response was significantly smaller, indicating no overall benefit when a stabilization step was introduced (Fig. 4d).

A comparison of *in-situ* vs. *ex-situ* immobilization was also executed, since the latter is more representative of the protocol used to prepare the WE in EGFET experiments. Between these two experiments, the peak RU value at  $10~\mu g/mL$  (890 nM) was over twice as high for the *in-situ* prepared surfaces (2417.6 RU) than the *ex-situ* surfaces (765.4 RU). Calculating the signal that can be attributed from the H4 proteins interaction with the aptamer was done by dividing the differential by the measured KU7+PEG response as a percent. The *in-situ* surfaces had 46.7% of the response from the aptamer and *ex-situ* was 65.8% at this concentration. Both protocols had some signal contribution from the PEG and confirmed that baseline stabilization is necessary for accurate EGFET measurements.

BSA and CTH SPR data is reported in the Supplementary Materials, Figs. S2–S6. Selectivity of the surface was achieved through BSA testing, where all active and control surfaces tested had no peak RU values larger than 25 RU. CTH showed diminished binding responses than that of H4. Trending similarly with the H4 response, *in-situ* preparation with 0hr storage had larger binding responses than 24hr storage. At 223 nM, *ex-situ* results showed an aptamer contribution of 60.5% compared to *in-situ* at 48.9%. A table with the kinetic binding constants for CTH is also in the Supplementary Materials as Fig. S7.

#### 3.3. Initial calibration of the EGFET platform to pH and ionic strength

The EGFET approach was first validated with PANI electrodes and showed the sensor's capability to detect large changes in  $V_{\rm GS}$  potential shifts through interactions with different pH buffers (e.g., pH 4, pH 7, and pH 10). The response was near-Nernstian with a sensitivity of 52.3 mV/pH (Fig. S8). For the ionic strength experiments, this setup allowed the EGFET system to measure [Cl $^-$ ] in the electrolyte directly and test how the salts and ions in the buffer impact the voltage response of the MOSFET channel. The platform was then tested with functionalized electrodes to understand the response to PBS with different ion concentration PBS buffer solutions. This was an important preliminary step since the device will have to operate in complex ionic media like whole blood. Understanding the effects of increasing ion content in a lab-controlled buffer will accelerate the progress of the system in

detecting histone proteins. Co-SAM electrodes were tested, starting with 1 mM PBS. The differential  $V_{GS}$  was plotted against the lowest ionic strength (Fig. 5a). This shift had a trend of  $-6.2\,\text{mV/mmol\,Cl}^-$  ions with  $R^2=0.98$ . The EGFET platform showed reliable testing for buffer and further ionic media will be tested in the future transition to human serum

Lastly, before transitioning to H4 human histone protein sensing, an aptamer and PEG electrode was prepared and subjected to multiple CTH solutions at varying ionic strengths. 200 nM CTH was measured to investigate the signal magnitude of CTH binding as a function of background electrolyte content. After the buffer measurements showed stabilization as described in Section 2.4, a new solution of 200 nM CTH was added to the batch cell. The differential was calculated between the CTH voltage and that of the corresponding strength buffer to show the voltage shift caused by biomolecule interactions, not the ionic content of the buffer. The voltage differentials for 200 nM CTH compared to the initial buffer measurements for each ionic strength are plotted with error bars representing the three measurements of the same CTH volume, each with four I–V sweeps. The CTH interactions caused a shift of 7.26  $\pm$  2.7  $\Delta$ mV, with the highest shift at 1.0x PBS (Fig. 5b). It was promising that significant potential shifts can be captured as the ionic background of the buffer or biofluid increases. It also provided some insight on the potential range of detection to expect moving to full concentration range

#### 3.4. EGFET results for H4, CTH, and BSA

H4, CTH and BSA were tested in a concentration range from 10 pM to 1  $\mu M$ . This range fully encompasses the expected 50 pM–200 pM pathophysiologic range of histone proteins in blood for healthy and inflamed individuals. This aptasensor had sensitive results with H4, achieving a lowest measured concentration of 10 pM, a sensitivity of 6.65 mV/dec ( $R^2=0.98$ ), and a calculated limit of detection (LOD) of 5 pM (Fig. 5c). CTH is a heterogenous mix of five major histone proteins and may have a structure that is not conducive to RNA aptamer sensing. CTH demonstrated a sensitivity of 3.05 mV/dec ( $R^2=0.94$ ) and a LOD of 800 pM with the concentration range of 1 nM to 1  $\mu M$ . LOD was calculated with LOD  $=3.3~{}^*\sigma/S$ , where S is the sensitivity of the data given by the logarithmic trendline and  $\sigma$  is the standard deviation of the lowest measured concentration (Lister et al., 2005). BSA as an interference molecule showed less than 5  $\Delta mV$  signal change at 100 nM and proved a 13x signal selectivity response for the H4 aptasensor.

#### 4. Discussion

## 4.1. Comparison of PEG and MCH as co-SAM spacer in SPR

Designing a sensor to operate in whole blood in the future while mitigating NSA and charge-screening effects requires strategic arrangement of aptamers on the surface to ensure they achieve a sufficient conformation change during binding. Differences in chemistry and electrostatic attraction of either MCH or PEG spacer molecules affect the steric hindrance of the aptamer and other intermolecular interactions, and thus impacts the measured sensor response of co-SAMs (Ricci et al., 2009). MCH is a small alkanethiol with a polar hydroxyl head group and a molecular weight of 134.237 Da. PEG has ether functional groups through the 2 kDa chain and a terminal methyl group most exposed to the histones in solution. The adoption of PEG in antifouling surfaces has been reported to prevent unwanted protein uptake due to its larger molecular weight creating a hydration layer (Li et al., 2023), (Liu et al., 2019)

As mentioned, Urak et al.'s SPR measurements with this aptamer sequence focused on the reverse system by using immobilized histones to detect aptamers in solution in order to corroborate the results of the SELEX process (Urak et al., 2019). In that case, aptamers exist with a quaternary folding structure while suspended in the solution. This

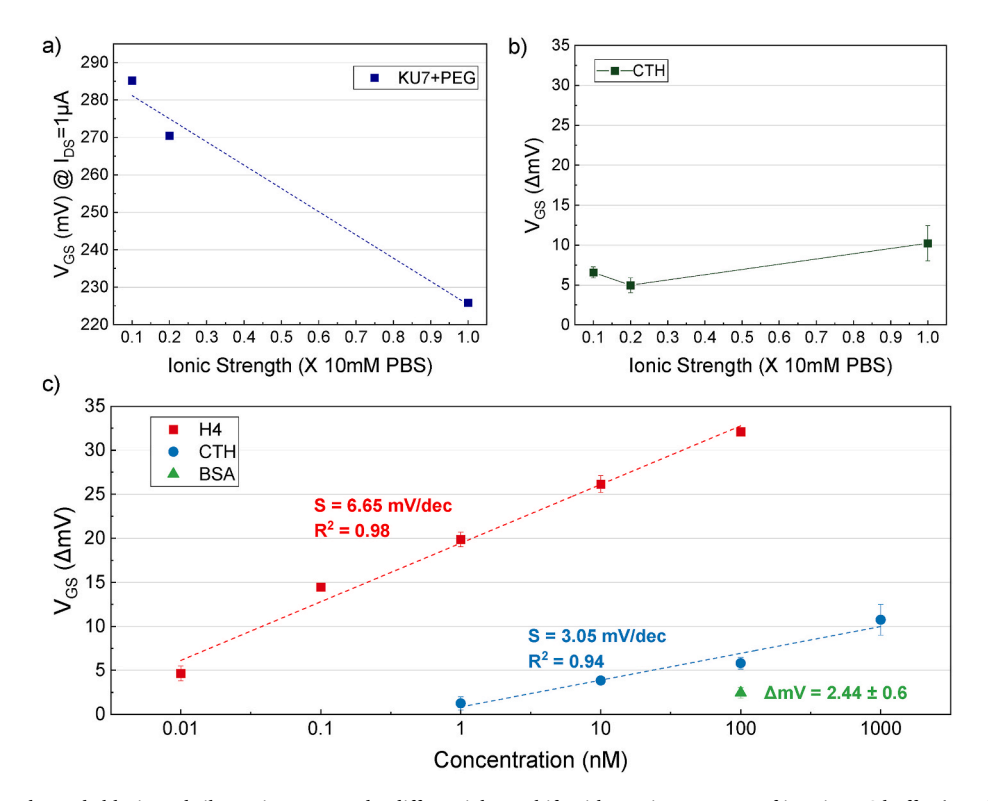


Fig. 5. a) Co-SAM electrodes and chlorinated silver wire measured a differential  $V_{GS}$  shift with varying amounts of ions in PBS buffer (n=8 sweeps). b) At different ionic strengths, 200 nM CTH was added and the differential  $V_{GS}$  calculated against PBS buffer (n=12 sweeps). c)  $\Delta V_{GS}$  response of H4, CTH, and BSA on anti-histone aptamer and PEG functionalized EGFET WEs (n=8 sweeps). (For interpretation of the references to colour in this figure legend, the reader is referred to the Web version of this article.)

structure is not possible in the desired EGFET sensor configuration due to one end being anchored to the gold with the thiol moiety (Fig. 1). Nonetheless, our SPR experiments confirm that anchored aptamers still successfully bind to H4 proteins.

SPR showed that both PEG and MCH exhibit some non-specific interaction with H4, but the differential signal (i.e., the difference between peak RU values in the active and control flow cells) was largest when PEG was used. The kinetic association ( $k_a$ ) and dissociation ( $k_d$ ) constants, as well as the equilibrium dissociation constant ( $K_D$ ) are reported in Table 1 for the binding for H4 (Ritzefeld and Sewald, 2011). The original SPR experiments by Urak et al. reported an estimated dissociative binding constant of  $K_D = 4.01$  nM. Here, for the *in-situ*, 0hr storage KU7+PEG co-SAM, a 1:1 binding method resulted in  $K_D = 7.68$  nM, which was near the SELEX results of the source publication. The 0hr storage method also proved beneficial when compared to case where 24hr storage is used ( $K_D = 9.49$  nM). The experiment using MCH showed the highest  $K_D$  of 56.23 nM, thus further emphasizing its incompatibility

**Table 1**Comparison of binding kinetic values for various SPR experiments.

Analyte	Ligand	Experiment	$10^4 \times k_a \ (M^{-1}s^{-1})$	$10^{-4}$ $\times k_d$ $(s^{-1})$	K <sub>D</sub> (nM)	Source
KU7	Н4	In-situ amine coupling	56.2	22.5	4.01	Urak et al. (2019)
H4	KU7 + MCH	<i>In-situ</i> , 0hr storage	0.303	1.70	56.23	This work
H4	KU7 + PEG	<i>In-situ</i> , 0hr storage	2.2	1.69	7.68	This work
H4	KU7 + PEG	In-situ, 24hr storage	2.56	2.43	9.49	This work
H4	KU7 + PEG	Ex-situ, 0hr storage	5.62	0.10	0.178	This work

within the anti-histone aptamer co-SAM.

When comparing the response to H4 obtained with *in-situ* immobilization to the case where *ex-situ* immobilization was used, it was found that *ex-situ* immobilization with 0hr storage had the lowest calculated  $\rm K_D$  value of 0.178 nM (Table 1). With CTH, this experiment measured an apparent  $\rm K_D=1.50$  nM (Fig. S6). Overall, the more complete survey of SPR experiments conducted in this work enabled binding constants below the maximum pathophysiological range of H4 histones (200 pM). This confirmed that the preparation of the WE functionalization when done outside of the SPR instrument was best for the sensor's operational concentration range, thus enabling bench-top EGFET measurements.

## 4.2. EGFET aptasensor for histone monitoring

Preliminary potentiometric measurements of aptamerfunctionalized surfaces for histone detection were reported previously (Richardson et al., 2022). There, the response was measured for concentrations of CTH from 1.56 nM to 1 µM in HBS-EP+ with a sensitivity of 7.8 mV/dec without the incorporation of a MOSFET. Here, we report EGFET-based sensitivity to CTH of 3.05 mV/dec with fabricated gold electrodes and improved calculated LOD of 800 pM. More importantly, however, in the case of H4 at picomolar levels, we achieve a sensitivity of 6.65 mV/dec, and a LOD of 5 pM. This is well below the physiological range of 50 pM-200 pM for healthy and high mortality patients, respectively. At 100 nM concentration, the potential shift for H4 binding was 32.1  $\pm$  0.4  $\Delta$ mV compared to only 2.4  $\pm$  0.6  $\Delta$ mV for BSA. The selectivity of the sensor towards H4 was 13:1 with respect to BSA. We achieve a larger output voltage shift in the nanomolar concentration range compared to previous reports using a DNA anti-histone aptamer in FET measurements (Goda and Miyahara, 2020). Thus, the EGFET results shown here for H4 are promising and show that sensing complications due to histone proteins' large molecular mass, high charge density, and high isoelectric point can be overcome with potentiometry and RNA aptamer technology.

Using the same EGFET measurement procedure, we also investigated the 24-h storage theory, demonstrating that the electrical sensitivity was also not improved (Fig. S9). Immediate testing of the prepared WE instead of storage optimized the histone binding with an improved increase in sensitivity, selectivity, and measurement stability. At this time, highest sensitivity was achieved when testing the sensor immediately following immobilization. Of course, future field deployment will require investigation of degradation mechanisms and stabilization solutions. The KU7 RNA aptamer has already been demonstrated to possess a 150-h half-life (Urak et al., 2019).

#### 5. Conclusions

We have established an EGFET platform capable of detecting pathophysiologic ranges of circulating human histone proteins. This biosensor has the potential to provide suitable POC identification of patients at an increased risk of rapid deterioration of their clinical status in future deployment studies. Gold working electrodes were prepared and characterized via a suite of tests. Through contact angle measurements and SPR, it was determined that the spacer used in the co-SAM impacts not only the target signal through NSA, but the ability of the aptamers to fold during binding to the analyte. This result was an improvement of our previous potentiometric measurements and underlines the importance of testing control surfaces in addition to specifically prepared active surfaces to quantify false signals and understand interfering interactions. A reduction in non-specific adhesion was made possible by substituting MCH for PEG for the best performance with the RNA aptamer recognition element. We report a sensitivity of 6.65 mV/dec and a LOD of 5 pM, for human histone H4. Selectivity studies demonstrated a signal that was 13-fold larger for H4 than for BSA, as a preliminary step towards testing the EGFET sensor tests in more complex media with competitive binding. Future studies may investigate alternative control surfaces to further reduce electrostatic interactions. Moreover, lifetime studies will be executed to identify opportunities for clinical deployment in the future for POC use.

# CRediT authorship contribution statement

Hayley Richardson: Writing – review & editing, Writing – original draft, Visualization, Validation, Software, Resources, Methodology, Investigation, Formal analysis, Data curation. Jeffrey Barahona: Writing – review & editing, Visualization, Software, Data curation. Greg Medwig: Visualization, Software. Angela Johns: Investigation, Data curation. Lina M. Acosta Pérez: Methodology, Writing – review & editing. Koji Sode: Resources, Methodology. Michael Daniele: Resources, Methodology. Francis J. Miller: Writing – review & editing, Supervision, Methodology, Funding acquisition, Conceptualization. Edgar Lobaton: Writing – review & editing, Supervision, Project administration, Methodology, Funding acquisition, Conceptualization. Spyridon Pavlidis: Writing – review & editing, Writing – original draft, Supervision, Resources, Project administration, Methodology, Funding acquisition, Formal analysis, Conceptualization.

#### Declaration of competing interest

The authors declare that they have no known competing financial interests or personal relationships that could have appeared to influence the work reported in this paper.

#### Data availability

Data will be made available on request.

#### Acknowledgements

The authors are grateful for the SPR expertise of Dr. Brian Watts and Dr. Kenneth Cronin at Duke University. Surface plasmon resonance analysis was performed in the Duke Human Vaccine Institute Biomolecular Interaction Analysis Shared Resource Facility (Durham, NC) under the direction of Dr. S. Munir Alam and Dr. Kenneth Cronin.

This work was supported by the U.S. National Science Foundation (NSF) via grants ECCS-1936772 (Pavlidis, Lobaton) and ECCS-2210335 (Miller) and the NSF Center for Advanced Self-Powered Systems of Integrated Sensors and Technologies (ASSIST) supported by grant EEC-116048. This work was performed in part at the NCSU Nanofabrication Facility (NNF) and the Analytical Instrumentation Facility (AIF) at North Carolina State University, which are supported by the State of North Carolina and the National Science Foundation (award number ECCS-2025064). The AIF is a member of the North Carolina Research Triangle Nanotechnology Network (RTNN), a site in the National Nanotechnology Coordinated Infrastructure (NNCI).

# Appendix A. Supplementary data

Supplementary data to this article can be found online at https://doi. org/10.1016/j.biosx.2024.100501.

#### References

- Arina, P., Singer, M., 2023. Chapter 8 diagnosis and monitoring of sepsis. In: Borges, M., Hidalgo, J., Perez-Fernandez, J. (Eds.), The Sepsis Codex. Elsevier, pp. 55–64. https://doi.org/10.1016/B978-0-323-88271-2.00037-7.
- Bain, C.D., Troughton, E.B., Tao, Y.T., Evall, J., Whitesides, G.M., Nuzzo, R.G., 1989. Formation of monolayer films by the spontaneous assembly of organic thiols from solution onto gold. J. Am. Chem. Soc. 111 (1), 321–335. https://doi.org/10.1021/ ia00183a049
- Bessière, A., Duhamel, C., Badot, J.-C., Lucas, V., Certiat, M.-C., 2004. Study and optimization of a flexible electrochromic device based on polyaniline. Electrochim. Acta 49 (12), 2051–2055. https://doi.org/10.1016/j.electacta.2003.12.034.
- Boon, E.M., Ceres, D.M., Drummond, T.G., Hill, M.G., Barton, J.K., 2000. Mutation detection by electrocatalysis at DNA-modified electrodes. Nat. Biotechnol. 18 (10), 1096–1100. https://doi.org/10.1038/80301.
- Cao, S., et al., 2023. ISFET-based sensors for (bio)chemical applications: a review. Electrochem. Sci. Adv. 3 (4), e2100207 https://doi.org/10.1002/elsa.202100207.
- Cho, E.J., Lee, J.-W., Ellington, A.D., 2009. Applications of aptamers as sensors. Annu. Rev. Anal. Chem. 2 (1), 241–264. https://doi.org/10.1146/annurev. anchem.1.031207.112851.
- Chu, C.-H., et al., 2017. Beyond the Debye length in high ionic strength solution: direct protein detection with field-effect transistors (FETs) in human serum. Sci. Rep. 7 (1), 5256. https://doi.org/10.1038/s41598-017-05426-6.
- Daniel, C., Roupioz, Y., Gasparutto, D., Livache, T., Buhot, A., 2013. Solution-phase vs surface-phase aptamer-protein affinity from a label-free kinetic biosensor. PLoS One 8 (9), e75419. https://doi.org/10.1371/journal.pone.0075419.
- Eckermann, A.L., Feld, D.J., Shaw, J.A., Meade, T.J., 2010. Electrochemistry of redoxactive self-assembled monolayers. Coord. Chem. Rev. 254 (15–16), 1769–1802. https://doi.org/10.1016/j.ccr.2009.12.023.
- Erb, R.A., 1968. Wettability of gold. J. Phys. Chem. 72 (7), 2412–2417. https://doi.org/ 10.1021/j100853a023.
- Gargano, A.F.G., et al., 2018. Increasing the separation capacity of intact histone proteoforms chromatography coupling online weak cation exchange-HILIC to reversed phase LC UVPD-HRMS. J. Proteome Res. 17 (11), 3791–3800. https://doi. org/10.1021/acs.jproteome.8b00458.
- Goda, T., Miyahara, Y., 2020. Label-free monitoring of histone acetylation using aptamer-functionalized field-effect transistor and quartz crystal microbalance sensors. Micromachines 11 (9), 9. https://doi.org/10.3390/mi11090820.
- Hatada, M., Pavlidis, S., Sode, K., 2024. Development of a glycated albumin sensor employing dual aptamer-based extended gate field effect transistors. Biosens. Bioelectron. 251, 116118 https://doi.org/10.1016/j.bios.2024.116118.
- Janićijević, Ž., et al., 2023. Methods gold standard in clinic millifluidics multiplexed extended gate field-effect transistor biosensor with gold nanoantennae as signal amplifiers. Biosens. Bioelectron. 241, 115701 https://doi.org/10.1016/j. bios.2023.115701.
- Josephs, E.A., Ye, T., 2013. Nanoscale spatial distribution of thiolated DNA on model nucleic acid sensor surfaces. ACS Nano 7 (4), 3653–3660. https://doi.org/10.1021/ nn400659m.
- Kaisti, M., 2017. Detection principles of biological and chemical FET sensors. Biosens. Bioelectron. 98, 437–448. https://doi.org/10.1016/j.bios.2017.07.010.
- Lei, B., et al., 2023. Inhalation of an RNA aptamer that selectively binds extracellular histones protects from acute lung injury. Mol. Ther. Nucleic Acids 31, 662–673. https://doi.org/10.1016/j.omtn.2023.02.021.

- Li, L., Yu, S., Wu, J., Ju, H., 2023. Regulation of target-activated CRISPR/Cas12a on surface binding of polymer dots for sensitive electrochemiluminescence DNA analysis. Anal. Chem. 95 (18), 7396–7402. https://doi.org/10.1021/acs. analchem.3c01521.
- Lister, A.S., 2005. Validation of HPLC methods in pharmaceutical analysis. In: Ahuja, S., Dong, M.W. (Eds.), Separation Science and Technology, Handbook of Pharmaceutical Analysis by HPLC, 6. Academic Press, pp. 191–217. https://doi.org/10.1016/S0149-6395(05)80051-0, 6.
- Liu, N., Xu, Z., Morrin, A., Luo, X., 2019. Low fouling strategies for electrochemical biosensors targeting disease biomarkers. Anal. Methods 11 (6), 702–711. https:// doi.org/10.1039/C8AY02674B.
- Liu, Y., Canoura, J., Alkhamis, O., Xiao, Y., 2021. Immobilization strategies for enhancing sensitivity of electrochemical aptamer-based sensors. ACS Appl. Mater. Interfaces 13 (8), 9491–9499. https://doi.org/10.1021/acsami.0c20707.
- Luo, J., et al., 2017. Early identification of patients at risk for acute respiratory distress syndrome among severe pneumonia: a retrospective cohort study. J. Thorac. Dis. 9 (10), 3979–3995. https://doi.org/10.21037/jtd.2017.09.20.
- Marshall, J.C., Cook, D.J., Christou, N.V., Bernard, G.R., Sprung, C.L., Sibbald, W.J., 1995. Multiple Organ Dysfunction Score: a reliable descriptor of a complex clinical outcome. Crit. Care Med. 23 (10), 1638.
- Nagata, M., Lee, J., Saito, T., Ikebukuro, K., Sode, K., 2023. Development of an antiidiotype aptamer-based electrochemical sensor for a humanized therapeutic antibody monitoring. Int. J. Mol. Sci. 24 (6), 6 https://doi.org/10.3390/ iims24065277
- Nuzzo, R.G., Allara, D.L., 1983. Adsorption of bifunctional organic disulfides on gold surfaces. J. Am. Chem. Soc. 105 (13), 4481–4483. https://doi.org/10.1021/ ia00351a063
- Purwidyantri, A., et al., 2015. Sensing performance of fibronectin-functionalized Au-EGFET on the detection of S. epidermidis biofilm and 16S rRNA of infection-related bacteria in peritoneal dialysis. Sensor. Actuator. B Chem. 217, 92–99. https://doi. org/10.1016/j.snb.2014.11.017.

- Rapsang, A., Shyam, D.C., 2014. Scoring systems in the intensive care unit: a compendium. Indian J. Crit. Care Med. 18 (4), 220–228. https://doi.org/10.4103/ 0972-5229 130573
- Ricci, F., et al., 2009. Surface chemistry effects on the performance of an electrochemical DNA sensor. Bioelectrochemistry Amst. Neth. 76 (1–2), 208–213. https://doi.org/ 10.1016/j.bioelechem.2009.03.007.
- Richardson, H., Maddocks, G., Peterson, K., Daniele, M., Pavlidis, S., 2021. Toward subcutaneous electrochemical aptasensors for neuropeptide Y. In: 2021 IEEE Sensors, pp. 1–4. https://doi.org/10.1109/SENSORS47087.2021.9639832.
- Richardson, H., Barahona, J., Carter, G., Miller, F.J., Lobaton, E., Pavlidis, S., 2022. Characterization of aptamer functionalized gold electrodes for histone detection. In: *Hilton Head 2022 Technical Digest*, Hilton Head, SC, USA, pp. 1–4.
- Ritzefeld, M., Sewald, N., 2011. Real-time analysis of specific protein-DNA interactions with surface plasmon resonance. J. Amino Acids 2012, 816032 [Online]. https://www.hindawi.com/journals/jaa/2012/816032/. (Accessed 27 October 2023).
- Szatmary, P., Huang, W., Criddle, D., Tepikin, A., Sutton, R., 2018. Biology, role and therapeutic potential of circulating histones in acute inflammatory disorders. J. Cell Mol. Med.
- Tarasov, A., et al., 2016. A potentiometric biosensor for rapid on-site disease diagnostics. Biosens. Bioelectron. 79, 669–678. https://doi.org/10.1016/j.bios.2015.12.086.
- Urak, K.T., et al., 2019. RNA inhibitors of nuclear proteins responsible for multiple organ dysfunction syndrome. Nat. Commun. 10 (1), 116. https://doi.org/10.1038/s41467-018-08030-y.
- Xiao, Y., Lai, R.Y., Plaxco, K.W., 2007. Preparation of electrode-immobilized, redox-modified oligonucleotides for electrochemical DNA and aptamer-based sensing. Nat. Protoc. 2 (11), 11 https://doi.org/10.1038/nprot.2007.413.
- Xu, J., et al., 2009. Extracellular histones are major mediators of death in sepsis. Nat. Med. 15 (11), 1318.
- Zuker, M., 2003. Mfold web server for nucleic acid folding and hybridization prediction. Nucleic Acids Res. 31 (13), 3406–3415.